



HAL
open science

Bulk properties of the Kondo-like system UCoGe

Robert Troc, Ryszard Wawryk, Wojciech Miiller, Halina Misiorek, Malgorzata Samsel-Czekala

► **To cite this version:**

Robert Troc, Ryszard Wawryk, Wojciech Miiller, Halina Misiorek, Malgorzata Samsel-Czekala. Bulk properties of the Kondo-like system UCoGe. *Philosophical Magazine*, 2010, 90 (16), pp.2249-2271. 10.1080/14786431003630900 . hal-00592297

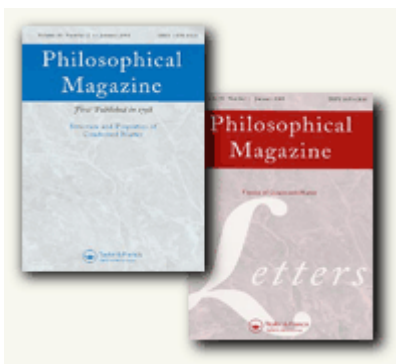
HAL Id: hal-00592297

<https://hal.science/hal-00592297>

Submitted on 12 May 2011

HAL is a multi-disciplinary open access archive for the deposit and dissemination of scientific research documents, whether they are published or not. The documents may come from teaching and research institutions in France or abroad, or from public or private research centers.

L'archive ouverte pluridisciplinaire **HAL**, est destinée au dépôt et à la diffusion de documents scientifiques de niveau recherche, publiés ou non, émanant des établissements d'enseignement et de recherche français ou étrangers, des laboratoires publics ou privés.



Bulk properties of the Kondo-like system UCoGe

Journal:	<i>Philosophical Magazine & Philosophical Magazine Letters</i>
Manuscript ID:	TPHM-09-Sep-0417.R1
Journal Selection:	Philosophical Magazine
Date Submitted by the Author:	12-Jan-2010
Complete List of Authors:	Troc, Robert; Institute of Low Temperature and Structure Research Polish Academy of Sciences, Department of Magnetic Investigation Wawryk, Ryszard; Institute of Low Temperature and Structure Research Polish Academy of Sciences Miiller, Wojciech; Institute of Low Temperature and Structure Research Polish Academy of Sciences Misiorek, Halina; Institute of Low Temperature and Structure Research Polish Academy of Sciences Samsel-Czekala, Malgorzata; Institute of Low Temperature and Structure Research Polish Academy of Sciences
Keywords:	actinides, superconductors, Kondo effect, thermal properties, transport properties, magnetoresistance, magnetization, electrical transport
Keywords (user supplied):	



Bulk properties of the Kondo-like system UCoGe

R. Troć*, R. Wawryk, W. Miiller, H. Misiorek, M. Samsel-Czekala

*Institute of Low Temperature and Structure Research, Polish Academy of Sciences,
P.O. Box 1410, 50-950 Wrocław 2, Poland*

* Author for correspondence. E-mail: r.troc@int.pan.wroc.pl; phone: (+48-71) 3435021 ext. 206; fax: (+48-71) 3441029

(Received 2009; final version received)

We report on extensive experimental investigation of a single crystal of the orthorhombic uranium compound UCoGe. Bulk measurements being done on as grown and annealed single crystals as magnetization, magnetic susceptibility, electrical resistivity, magnetoresistivity, thermopower, thermal conductivity, and heat capacity data do not reproduce the previously reported coexistence of ferromagnetism with superconductivity. The latter phenomenon was only observed for the annealed sample with $T_{SC} = 0.65$ K. Quite new observations are a crossover at around 13 K visible in thermal and transport measurements as well as the coherent state around 50 K signaled by a wide knee in $\rho(T)$. Above this temperature UCoGe exhibits a single-ion Kondo-like effect. The magnetoresistivity of the annealed single crystal is increasing negatively down to 4.2 K, reaching as a large value as about -27% at a field of 8 T. The latter may be interpreted in terms of fairly strong magnetic fluctuations existing in UCoGe at low temperatures.

PACS numbers: 74.25.-q, 74.25.Ha, 75.20.Hr, 75.47.-m

1. Introduction

The various *UTM* ternaries (T = transition metal) with $M = \text{Si}$ and Ge were first prepared by arc melting many years ago [1]. Their orthorhombic crystal structure, mainly of the TiNiSi -type (space group: $Pnma$) with the U atoms arranged in characteristic zigzag chains along the a axis, as well as the magnetic properties were recognized. A rule of thumb was found, stating that together with reducing the d-electron occupation the magnetism weakens and magnetic ordering disappears [1,2]. Considering only the germanide series, three of them, namely UFeGe [3], UCoGe and URuGe [1] with reduced d-electron occupation have just been found to be paramagnetic down to 4.2 K. The remaining studied compounds in this series, namely

1
2
3 with $T = \text{Rh, Ir, Ni, Pd and Pt}$, are magnetically ordered, exhibiting a gradual growth
4 of their transition temperatures with increasing U-U distances [1]. Furthermore,
5 magnetization measurements performed for all this series, except for UFeGe, in high
6 magnetic fields up to 38 T at 4.2 K, confirmed the paramagnetic properties of UCoGe
7 and URuGe [2]. This systematics is apparently connected with the expected
8 tendencies to yield an increase in the 5f-ligand hybridization (besides the 5f-5f
9 overlap favored by small U-U separations) with decreasing the U-U distances
10 gradually delocalizing the 5f-electrons and in consequence leading to destabilizing the
11 uranium magnetic moments. For example, by applying high magnetic fields at low
12 temperatures in the case of UCoGe one first observes a linear behavior between 5 and
13 10 T and then a slight convex curvature of the magnetization with a field induced
14 magnetic moment as large as $0.58 \mu_B$ at 35 T [2,4]. This indicates quite obviously that
15 UCoGe is probably close to a ferromagnetic (FM) order, *i.e.*, it might reveal the
16 proximity to a quantum critical point (QCP). Precisely on such a border of FM order
17 one can expect in this compound superconducting (SC) behavior mediated by critical
18 magnetic fluctuations with the possible pairing of electrons into a spin triplet state [5].
19 Previously for UCoGe the absence of a magnetic order down to 1.2 K was reported,
20 and an appreciable value of the linear specific-heat coefficient $\gamma(0 \text{ K})$ of 65 mJ K^{-2}
21 $\text{mol}^{-1} \text{ U}$ was established in UCoGe through specific heat measurements [4]. The
22 electronic structure of these materials—being strongly depending on the occupation of
23 the d-electron shell—indicates that the narrow 5f-band is located near or at the Fermi
24 level, E_F , as is visible in recently published brief reports on possible weak
25 ferromagnetism in UCoGe in Refs. [6], [7] and [8] containing band structure
26 calculation results based on the full relativistic full potential local-orbital (FPLO)

1
2
3 minimum basis code [9] within the local (spin)-density approximation (L(S)DA), used
4
5 in [6,8], and the WIEN2k package within L(S)DA [6] as well as LSDA+*U* [7]
6
7 methods.
8
9

10
11 Recently a number of papers [10-18] have indicated the co-existence of weak
12
13 ferromagnetic (FM) and SC states in UCoGe below the critical temperature, $T_S = 0.5$
14
15 – 0.7 K. The p-wave type of superconductivity and an axial SC state with nodes along
16
17 the easy magnetization direction along the *c* axis was postulated [10]. Very recently a
18
19 weak itinerant FM order has been detected in zero-field muon-spin rotation (μ SR)
20
21 measurements [16]. As the authors of Ref. [16] declared, the μ SR study provides an
22
23 unambiguous proof for ferromagnetism present in the whole sample volume of the
24
25 above germanide confirming the conclusions of earlier papers about the coexistence
26
27 of ferromagnetism with superconductivity on the microscopic scale. Ferromagnetic
28
29 quantum critical fluctuations (FM-QCF) and anomalous coexistence of
30
31 ferromagnetism and superconductivity in UCoGe have been revealed also by Co-
32
33 NMR and NQR studies on a powder sample [17]. As a source of superconductivity in
34
35 UCoGe the proximity of the system to the FM-QCP has been suggested. Interestingly,
36
37 a high-pressure study of a single-crystalline UCoGe has recently revealed [18] that
38
39 ferromagnetism is smoothly depressed and near the FM critical point
40
41 superconductivity is enhanced to a maximum ($T_S = 0.60$ K) at 1.11 GPa and is still
42
43 present in the paramagnetic phase at pressures even above 2 GPa. Because of a
44
45 limitation to only low temperature studies of all cited works [10-18] published on the
46
47 above germanide up to now, we report here a set of new observations of the magnetic,
48
49 transport and thermal properties in most cases for the first time given in a wide
50
51 temperature range, measured also on a single-crystalline sample of UCoGe.
52
53
54
55
56
57
58
59
60

2. Experiment and calculations

The single crystal having a shape of a cylinder of dimensions $l = 5.0 \text{ mm} \times \phi = 1.5 \text{ mm}$ was grown by the Czochralski technique at the University of Silesia. The starting elements (with purity in weight percent) were: U (99.98), Co (99.99), and Ge (99.999). The quality of the single crystal before annealing (called as grown sample) was not high as indicates its temperature dependence of the resistivity (see below). The situation was completely changed after annealing the as grown sample at **900 K** for 7 days in a high vacuum.

Magnetization and magnetic susceptibility measurements have been performed using a commercial superconducting quantum interference device (SQUID) magnetometer in the temperature region from 1.72 K up to 400 K and in fields up to 5 T. The electrical resistivity measurements were performed using a steady-current four-point method with spot-welded wire contacts on cylindrically-shaped specimen at temperatures between 0.3 K and 300 K and in transverse magnetic fields ($\mathbf{j} \perp \mathbf{B}$) up to $B = \mu_0 H = 8 \text{ T}$. The geometrical factor of the sample was determined with accuracy not lower than 20%. The thermoelectric power in the low temperature range (0.4 - 50 K) and at the higher temperatures from 40 K to 360 K has been measured as described in Refs. [19,20], respectively. For thermoelectric power examinations the specimens were cut out to the dimensions of about $2.5 \times 1 \times 1 \text{ mm}^3$ along the cylinder axis, being the [001] direction of the crystal. The temperature difference (ΔT) at lowest T was kept of the order 0.3 K along the sample while above 20 K $\Delta T \cong 2 \text{ K}$. The thermal conduction was probed using the stationary heat flux method in the temperature range 5 - 300 K. The difference ΔT along the sample was

1
2
3 in the range 0.1-0.5 K. Particular care was taken to avoid a parasitic heat transfer
4 between the sample and its environment. Specific heat measurements in the
5 temperature range from 0.35 to 180 K were performed in a commercial multi-purpose
6 measurement device (Quantum Design PPMS) with a 2τ -relaxation-type method.
7
8
9

10
11
12 For the purpose to estimate diffusion term of thermoelectric power, we used
13 the densities of states (DOS) of UCoGe that has been reported and discussed in [8].
14 They were calculated by employing the fully relativistic version of the FPLO method
15 [9] in which the 4-component Kohn-Sham-Dirac equation, containing implicitly spin-
16 orbit coupling up to all orders, is solved self-consistently. The Perdew-Wang
17 parametrization [21] of the exchange-correlation potential in the LDA approach was
18 utilized. In the calculations the experimental values at room temperature of lattice
19 parameters and atomic positions in the unit cell were used from tables 1 and 2 in [8].
20 The adopted valence basis sets were as follows: the U: 5d5f;6s6p6d;7s7p, Co:
21 3s3p3d;4s4p and Ge: 3s3p3d;4s4p states. The size of the \mathbf{k} -point mesh of 12 x 12 x12
22 in the Brillouin zone turned out to be sufficient.
23
24
25
26
27
28
29
30
31
32
33
34
35
36
37
38
39

40 **3. Results and discussions**

41 **3.1. Magnetic properties**

42
43
44
45
46 The susceptibility data of UCoGe were measured in a field of 0.5 T along the
47 cylindrical axis of the sample and perpendicular to it, which are approximately
48 equivalent to the directions parallel, and perpendicular, respectively, to the
49 crystallographic c axis χ_i (i means $\mathbf{B} \parallel c$ and $\mathbf{B} \perp c$). Figure 1(a) shows the temperature
50 change of magnetic susceptibilities measured in these two directions for both kinds of
51 samples, *i.e.*, as grown and annealed ones. As seen from this figure, the differences
52
53
54
55
56
57
58
59
60

1
2
3 between the $\chi_i(T)$ curves obtained for the same sample but after different thermal
4 treatment are negligible in the whole temperature range of measurements (shown are
5 only data determined up to 100 K). It means that these various treatments of the
6 sample do not influence so much its magnetic behavior. Note, however, an existing
7 pronounced anisotropy in the magnetic behavior between these two orientations of a
8 single crystal. No sign of the susceptibility saturation in approaching $T=0$ K is
9 apparent. In the inset of this figure, we have presented the field dependence of the
10 magnetization \mathbf{M} (in μ_B) in applied fields $\mathbf{B}||c$ up to 5 T taken at various temperatures
11 from 1.72 to 25 K. One can see pronounced curvatures of this dependence
12 diminishing with increasing temperature up to 25 K, but without remanence M_0 at
13 each temperature measured. The lack of the field dependence of the susceptibility
14 appears only above this temperature giving rise to a normal paramagnetic behavior.
15 So that the FM correlations in UCoGe start to develop below 20 K, which is well
16 evidenced from the inset of figure 1(a). This is a clear sign of an existence of only
17 strong magnetic correlations in this annealed sample over this temperature range. The
18 induced magnetic moment at 1.72 K in a field of 5 T is equal to $0.14 \mu_B$. A very
19 similar magnetization dependence at the same temperature region (not shown) is
20 noted also for $\mathbf{B} \perp c$ but with lower induced moments at 5 T. For purpose of a
21 comparison, we have also plotted in this inset the magnetization curve measured by
22 Huy *et al.* [9] (solid line) on a single crystal of UCoGe at 2 K oriented along the c -
23 axis. In contrast to our results, this curve displays the ferromagnetic behavior due to
24 the presence of a spontaneous magnetization M_s with a value of $0.07 \mu_B$. The total
25 (intrinsic and induced) moment at 5 T was found to be about $0.21 \mu_B$. After
26 subtracting the value of their M_s one obtains the same value of the induced moment
27
28
29
30
31
32
33
34
35
36
37
38
39
40
41
42
43
44
45
46
47
48
49
50
51
52
53
54
55
56
57
58
59
60

found in our work. In order to better emphasize the behavior of the magnetization M , in figure 1(b) we have plotted the Arrott diagram (i.e. $\mu_0 H/M$ vs. M^2) at fixed temperatures from 1.72 K up to 25 K. The isotherms that intersect the M^2 axis indicate usually the presence of a spontaneous magnetization. In our case such an intersect is negligible and unusual only at 1.72 K. A typical Arrott diagram should show linear isotherms, also that intersecting the origin of the coordinate system, which in the case of a ferromagnet indicates the T_C temperature, as it was shown for the polycrystalline samples in Refs. [10] and [11]. As seen in figure 1(b), the above dependence measured at 1.72 and 5 K in higher values of $\mu_0 H/M$ are almost identical to each other, but in lower values of $\mu_0 H/M$ both show a strong curvature due to a substantial magnetic correlation effect and any T_C can not be detected.

The temperature dependences of the inverse molar susceptibility along the above directions are displayed in figure 2. The obtained $\chi^{-1}_i(T)$ curves showing pronounced curvatures in all the temperatures measured can be fitted in the temperature range 100 – 400 K to the modified Curie-Weiss (MCW) law (denoted by the dashed lines) with the parameters given in the figure. Below about 100 K the temperature derivatives of the $\chi^{-1}_i(T)$ curve become gradually increasing compared to the fitted MCW curves and, thus, this function diverges from the MCW fit

$\chi^{-1}(T) = [\chi_0 + N_A \mu_{eff}^2 / 3k_B (T - \Theta_p)]^{-1}$ where χ_0 , N_A , k_B , μ_{eff} , and Θ_p have usual meaning. From the point of view of the crystal electric field (CEF) theory such a rapid χ^{-1}_i vs. T bending can be easily explained by thermal depopulation of CEF levels with decreasing temperature. In the case of the $5f^2$ configuration of uranium atom one should expect rather a saturation tendency of these curves to a constant value at low temperatures (Van-Vleck paramagnetism) due to the low symmetry of the

1
2
3 orthorhombic crystal structure of UCoGe yielding only CEF singlets. The observed
4 curvature could be, however, well explained by the $5f^3$ uranium electronic
5 configuration for which in this symmetry Kramer's doublets arise. However, one can
6 not exclude the influence of the paramagnetism of Co atoms. As some paramagnetic
7 data for several ternary uranium compounds containing cobalt indicate (see for
8 example cases of UCoAl and its solid solutions with Ni [22, 23] and U_2CoSi_3 [24]) a
9 strong curvature of their $\chi^{-1}_i(T)$ takes place. It should be mentioned that the obtained
10 high temperature results are in reasonable accordance with the previous data
11 published in Ref. [1]. There is, however, some difference in the effective magnetic
12 moments between our present value $\mu_{\text{eff}} = 1.98(5) \mu_B$ (this paper) and that given in
13 Ref. [12] of $1.6(1) \mu_B$ (no curve is shown). A similar curvilinear behavior of $\chi^{-1}_i(T)$
14 has been reported for the solid solutions of the polycrystalline $U(Co_{1-x}Ru_x)Ge$
15 samples for $x = 0.4 - 1.0$ (see Ref. [11]) measured in a field $B = 1$ T in the
16 temperature range $2 - 300$ K. In the upper inset of figure 2 we show the temperature
17 variation of the magnetization $\sigma_i(T)$ taken at 0.5 T while in the lower inset we display
18 a field dependence of the magnetization $M_i(B)$ measured only at 1.72 K. As seen, in
19 our case the curvilinear decrease in $M_a(B)$ observed down to 0 K for both
20 orientations of the sample is without hysteresis, *i.e.*, no magnetic remanence exists.
21 Therefore, it can be related only to the presence of ferromagnetic correlations (FMC)
22 in contrary to having the spontaneous moment observed earlier on both the
23 polycrystalline [10,12] ($0.029 \mu_B$) and single-crystalline [13] ($0.07 \mu_B$) samples. The
24 upper inset of figure 2 reveals only a negligible change in a slope of these two curves
25 at the temperature expected for the ferromagnetic transition $T_C = 3$ K.
26
27
28
29
30
31
32
33
34
35
36
37
38
39
40
41
42
43
44
45
46
47
48
49
50
51
52
53
54
55
56
57
58
59
60

3.2 Transport properties

3.2.1 Resistivity and magnetoresistivity

The electrical resistivities measured previously by different authors on the polycrystalline and single-crystalline samples of UCoGe have been presented so far only in the small ranges of low temperatures, namely between 0.02 – 8 K [10], 0.23 – 10 K [12,13], 0.4 – 8 K [14] and 0.25 – 10 [15]. Contrastingly, we present in figure 3 the temperature dependences of the resistivity measured in a wide temperature range, *i.e.*, between 0.3 and 300 K for both kinds of UCoGe samples.

As is apparent in figure 3, the quality of our single crystal before annealing was not so high. The transport measurement data show rather a poor residual resistivity ratio RRR of about 2. It seems that this was mainly caused by a small deviation of the *c* axis of crystallites from the cylinder axis yielding an additional electron scattering on the crystallite separations. It appears, however, that the quality of the same single crystal, but annealed at 900 K for one week, has been distinctly improved by reaching the RRR ratio of 19. The resistivity data of this annealed sample are also plotted against temperature in this figure. Nevertheless, despite the difference in the absolute magnitudes of the resistivity, especially at low temperatures, and the lack of the superconductivity down to 0.3 K for the non-annealed sample, the temperature characteristics of the resistivity for both samples have almost identical features, as shown in the insets to figure 3. In contrast to the previously published data reported by other authors, both these samples exhibit at low temperatures the linear $\rho(T)$ dependence and, in addition, the inflection point T_{inf} at about 13 K with further linear behavior when the temperature is increased above this

1
2
3 point (see the left hand inset of figure 3). An analogous electrical behavior measured
4
5 up to 25 K on polycrystalline UCoGe has recently been reported by Huy and de
6
7 Visser [25]. In turn, in the right hand inset of figure 3 the temperature derivative of
8
9 the resistivity is plotted against the temperature. For both samples a wide maximum
10
11 around T_{inf} is well apparent underlining strongly the fact that at this temperature there
12
13 is a *crossover* probably dividing the energy scale for the here-studied compound into
14
15 low-temperature and higher temperature regions. The aforementioned linearity is
16
17 better seen on an enlarged picture of the low-temperature curve of $\rho(T)$ presented in
18
19 figure 4, where also no sign of a distinct anomaly around 3 K is observed, *i.e.*, at the
20
21 temperature claimed as a Curie point for the polycrystalline and single-crystalline
22
23 samples studied by other authors (see Refs. [10-18]). Recently, such a linear behavior
24
25 above the corresponding T_{sc} 's has been found in the super clean samples of URu₂Si₂
26
27 [26] and NpPd₅Al₂ [27]. Also for the URh_{0.62}Ru_{0.38}Ge solid solution lying on the
28
29 border of ferromagnetism the non-Fermi liquid (NFL) regime has been reported [28].
30
31 Thus, in the latter U(Rh,Ru)Ge system the randomness interactions between localized
32
33 and itinerant electrons acting near the critical concentration $x_{\text{cr}} \approx 0.38$ are thought to
34
35 be an origin of a NFL behavior (see e.g. Ref. [29]), supported also by the low-
36
37 temperature $C_p \sim T \ln T$ dependence [30].
38
39
40
41
42
43
44
45

46 On the contrary, the T^2 Fermi liquid law has been reported in all cases
47
48 mentioned above [10-14, 25]. In Ref. [15] The T^2 dependence is reported below T_C
49
50 and $T^{5/3}$ above this temperature up to 10 K. Since all these samples were weakly
51
52 ferromagnetic at low temperatures, such a behavior was explained, e.g., in Ref. [12]
53
54 by scattering on magnons with the same exponent. Figure 4 also clearly illustrates the
55
56 SC transition at $T_{\text{SC}} = 0.65$ K. Furthermore, in the next figure 5 we show the
57
58
59
60

1
2
3 difference $\Delta\rho_i$ ($\rho - \rho_0$), where ρ is a measured resistivity and ρ_0 is the residual one,
4 plotted against temperature for the annealed sample of UCoGe ($\Delta\rho_1$) and for reference
5
6 sample of ThNiGe ($\Delta\rho_2$). We have not used here as a reference, e.g., ThCoGe because
7
8 the latter compound exhibits some weak ferromagnetic behavior up to about 200-250
9
10 K, as we and the authors of Ref. [31] have found. The crystal structure of these two
11
12 Th-based ternaries is, however, of the hexagonal AlB₂-type and, therefore, both these
13
14 ternaries are not isostructural with the orthorhombic TiNiSi-type of UCoGe, but at
15
16 present no other possibility exist to use a better reference material.
17
18
19
20
21

22 As a result of using the non-magnetic reference we display in figure 5 the
23
24 resulting curve for UCoGe ($\Delta\rho_{1,2} = \Delta\rho_1 - \Delta\rho_2$) which distinctly shows the Kondo-like
25
26 behavior above about 80 K. As is also clear from this figure, as well as from figure 6,
27
28 where we plotted the above difference in a manner $\Delta\rho_{1,2}$ vs. $\log T$, the high
29
30 temperature Kondo-like effect is preceded by a knee in these curves. The maximum as
31
32 observed above, marked as T_{coh} , is usually associated with the coherence effect in the
33
34 Kondo-lattice system [32]. The fitting parameters are also shown in this figure.
35
36
37
38

39 The measured overall temperature dependence of the electrical resistivity of
40
41 UCoGe resembles that of other intermetallic uranium ternaries, but especially that of
42
43 URu₂Si₂ [34]. In a similar way to the case of URu₂Si₂, our $\Delta\rho_{1,2}(T)$ decreases also
44
45 rapidly below 50 K down to a residual resistivity at its superconducting temperature.
46
47 Previously, the only existing $\rho(T)$ curve, obtained for UCoGe in a wide temperature
48
49 range 1.5 – 300 K, has been reported by Canepa et al. [35]. Despite annealing of their
50
51 polycrystalline sample (at 1250 K for 3-5 days), the overall resistivity values given by
52
53 them are almost one order of magnitude larger than those of our annealed sample.
54
55 Moreover, the latter authors observed some sharp maximum in their $\rho(T)$ at $T_{\text{max}} = 46$
56
57
58
59
60

1
2
3 K instead of our smooth “knee”, which they interpreted as an evidence of non-
4
5 identified magnetic transition at this temperature.
6
7

8 Additionally, in the inset to figure 6 we have plotted the temperature
9
10 dependence of the resistivity for ThNiGe with fitting these experimental results into
11
12 the modified Bloch-Grüneisen-Mott equation [33] allowing to determine the Debye
13
14 temperature Θ_D^R (=139 K) for this compound. Our overall results of the resistivity
15
16 found for this Ni-based ternary material is by a factor of about 5 lower than those
17
18 published in the literature [31].
19
20
21

22 Finally, in figures 7 (a) and 7 (b) the low temperature resistivity $\rho(T)$,
23
24 measured in fields $B= 0$ and 8 T as well as transverse magnetoresistivity (TMR),
25
26 defined as $\Delta\rho/\rho = [\rho(B,T) - \rho(0,T)]/\rho(0,T) \times 100$ (%) are shown, respectively. If for
27
28 $B= 0$, as indicated above, this former dependence is linear in temperature, the
29
30 situation is changed into the Fermi liquid (FL) behavior at 8 T (see the inset of figure
31
32 7(a)). So that the FL state has been recovered in applied magnetic fields. In figure
33
34 7(b), where we have plotted the $\Delta\rho/\rho(T)$ curve below 60 K measured at 8 T, a strong
35
36 negative increase in TMR with lowering T is apparent with an appearance of a sharp
37
38 negative minimum at 8 K which reason is at present unknown. Furthermore, as the
39
40 inset to this figure clearly shows, the characteristic temperature T_{inf} is marked at
41
42 about 13 K, i.e. exactly at the same temperature as found from the temperature
43
44 derivative of the resistivity as the *crossover* temperature described above.
45
46
47
48
49
50

51 Next, we show in figure 8 the TMR as a function of a field B (applied up to 8
52
53 T) taken at different temperatures (4.2 – 40 K). For all temperatures measured we
54
55 have obtained the negative dependences of TMR, which character, however, changes
56
57 with decreasing temperature. It appears that this is typical of the Kondo-lattice-like
58
59
60

1
2
3 behavior (convex curve) at temperatures above 15 K, but below this temperature it
4 becomes an S-shaped one in the range of 15 – 10 K to become, finally, almost
5 concave in fields at 4.2 K as is expected for a ferromagnet. At the latter temperature,
6 $\Delta\rho/\rho(B)$ achieves the large negative overall value up to 8 T, where it attains about –25
7 %, however it still increases negatively up to -28 % reaching its maximum at about 8
8 K. The character of field and temperature dependencies of the as grown sample of
9 UCoGe was analogous, but the maximum value of TMR was found by a factor of 2.8
10 lower (-10%). The increase in the absolute value of TMR with lowering the
11 temperature, as is presented in figure 8, indicates that down to almost T_{inf} an expected
12 Kondo-lattice-dependence takes place. A change in the observed overall slopes gives
13 rises to the *crossover* around 13 K mentioned above. The dashed lines illustrate the -
14 $\alpha(\mu_0H)^2$ dependencies with the α coefficient varied with temperature.

3.2.2 Thermoelectric power

35
36 The measured Seebeck coefficient $S(T)$ of UCoGe is displayed in figure 9. As seen,
37 the main feature of this curve is a pronounced positive maximum at $T_{\text{max}} = 13$ K which
38 coincides well with the temperatures of maxima in the temperature derivatives of both
39 the resistivity (right hand inset of figure 3) or magnetoresistivity (insert of figure 7(b))
40 and also with T_{max} of the smaller peak in $\Delta C_p(T)$ (see below the inset of figure 12(b)).
41 As we have pointed out in the previous sections of this paper, this temperature is in
42 our system under study a measure of the characteristic *crossover* temperature, denoted
43 as T_{inf} . In the case of thermoelectric power (TEP) such a maximum in $S(T)$ can often
44 be interpreted as being due to the Kondo lattice effect [36], where $T_{\text{max}} = T_K/3$ or for
45 very clean samples as a phonon drag effect [37]. However, the latter should take place
46
47
48
49
50
51
52
53
54
55
56
57
58
59
60

1
2
3 at about $\Theta_D/10$, *i.e.*, at about 25 K for $\Theta_D= 248$ K being the Debye temperature
4
5 derived in the low temperature region of the specific heat of UCoGe (see lower inset
6
7 of figure 12(a)). On the other hand, the TEP of UCoGe resembles the behavior of
8
9 superconducting, spin fluctuating UPt₃ [38,39], where the positive peak at $T \sim 8$ K is
10
11 considered as a measure of the spin fluctuation temperature T_{sf} . It should be also
12
13 mentioned here that a very similar TEP and resistivity behavior exhibits U₃Au₃Sn₄
14
15 [40], which is considered as a heavy fermion system with $\gamma(0)= 280$ mJ K⁻² mol⁻¹ U.
16
17
18
19
20 The large γ value is predominantly caused by a reduced f-d hybridization.
21

22 Furthermore, according to the phenomenological model which considers
23
24 scattering conduction electrons by the 5f quasi-particle band of a Lorentzian form,
25
26 used in Ref. [41] at higher temperatures for the TEP results of correlated cerium and
27
28 uranium systems, $S(T)$ can be described using the following equation: $S(T)= A_i T/(B_i^2$
29
30 $+ T^2)$, where $i= N$ or W in the case of a narrow or wide band of the 5f electrons,
31
32 respectively. From a fitting of this equation to the low temperature $S(T)$ results we
33
34 can estimate roughly the f-electron level position to the Fermi level, $\Delta= \varepsilon_f - E_F$, and
35
36 the width Γ of the band in a Lorentzian form, because $A_N = 2\Delta/|e|$ and $B_N^2 = 3(\Delta^2 +$
37
38 $\Gamma^2)/(\pi k_B)^2$. As shown in the lower inset of figure 9, the TEP peak in UCoGe can be
39
40 well fitted by the narrow, single Lorentzian band (SLB) model, but only up to 30 K.
41
42 Above this temperature, the theoretical curve diverges upward from the experimental
43
44 one. This deviation from the SLB model observed at higher temperatures may be
45
46 connected with scattering processes that are beyond this model, like a phonon-drag
47
48 effect (see below), crystal field interactions, and so on. For the parameters A_N and B_N
49
50 given in the inset we find $\Delta= 0.26$ meV and $\Gamma= 2$ meV. This might indicate that in
51
52 UCoGe we have to do with more localized character of the 5f-electrons which,
53
54
55
56
57
58
59
60

1
2
3 however, below the *crossover* temperature become more itinerant. The latter is also
4 consistent with the linear behavior of $S(T)$ characteristic of normal metals as is
5
6 observed for UCoGe below about 2.5 K (upper inset of figure 9). According to the
7
8 equation followed by metals: $S(T) = \alpha T$, where $\alpha = \pi^2 k_B / 3 |e| T^*$, in our case $\alpha \sim 2.8 \mu\text{V}$
9
10 K^{-2} which yields $T^* \sim 100 \text{ K}$, just as the value T_K , determined from the Kondo-like
11
12 peak in the specific heat (see figure 12(b) and the corresponding text). The value α is
13
14 practically the same for both kinds of samples used in our studies, so that we present
15
16 in figure 9 only the results obtained on the as grown sample. The difference between
17
18 TEPs in these two samples, except for a small difference in their magnitudes, is well
19
20 seen only below about 0.8 K where the annealed sample starts to go into the SC state,
21
22 where TEP drops to 0.
23
24
25
26
27
28

29
30 In order to estimate an overall magnitude of the temperature dependence of
31
32 TEP in UCoGe, we have applied the Mott model for diffusion TEP, $S_d(T)$, of a two-
33
34 band conductor [42] in an analogous manner as it was done for UCoGa₅ in Ref. [43]
35
36 using the following formula:
37
38

$$39 \quad S_d(T) = \frac{\pi^2 k_B^2 T}{3e} \left\{ \left[\frac{1}{N_s(E)} \frac{dN_s(E)}{dE} \right]_{E=E_F} - \left[\frac{1}{N_{pdf}(E)} \frac{dN_{pdf}(E)}{dE} \right]_{E=E_F} \right\}, \quad (1)$$

40
41 where N_s and N_{pdf} denote the sums of contributions to densities of states coming from
42
43 all conduction electrons, i.e s and p, d, f ones, respectively. We used our calculated,
44
45 employing the FPLO code [9] in the LDA approach, N_s and N_{pdf} densities in
46
47 paramagnetic UCoGe, reported in [8], and computed their derivatives over energy at
48
49 E_F , being presented in figure 10. As is seen in this figure, the N_s contribution in
50
51 UCoGe is equal to 0 (see triangles), thus also its derivative. Hence, only the second
52
53 term connected with the N_{pdf} density remains non-zero in the above equation. In this
54
55
56
57
58
59
60

1
2
3 way, we obtained the linear dependence of diffusion TEP as follows: $S_d(T) = -$
4
5 $14.7 \times 10^{-2} T$ ($\mu\text{V K}^{-1}$), which is plotted in figure 9 (dashed straight line). It is seen that
6
7
8 the calculated $S_d(T)$ yields a negative linear temperature variation reflecting the
9
10 general trend of the experimental TEP at higher temperatures.
11

12
13 It is interesting to add that in the case of the strong scattering of phonons by
14
15 electrons, which has been noted in connection with the thermal conductivity of
16
17 UCoGe considered below, the TEP comprises mainly diffusion S_d and a phonon drag
18
19 S_{ph} contributions. If one takes the former one, $S_d(T)$, being negative in the whole
20
21 temperature region studied, just as that found from the above calculations, then the
22
23 latter, $S_{ph}(T)$, should have only positive values, and their sum $S_d(T) + S_{ph}(T)$, would
24
25 give the resulting shape of our measured TEP depicted in figure 9. Such an approach,
26
27 *e.g.*, has been proposed for the superconducting cuprates [44] and could also be
28
29 applied in our case, but it requires at least to perform neutron inelastic scattering
30
31 measurements on a large single crystal of UCoGe. It turned out, that for several
32
33 uranium compounds, like UNi_4B , UPt_2In , and $\text{UCu}_{3+x}\text{Ga}_{2-x}$ as well as for UNi_2Al_3 and
34
35 UPd_2Al_3 , two 5f-band Mott's Lorentzian model, where both $i = N$ and W cases had to
36
37 be used together. Thus, this signals the presence of two energy scales in these
38
39 systems. It is common, however, for all these materials that their TEP increases with
40
41 an upward curvature, *i.e.*, in an opposite way to the TEP of UCoGe, and with a
42
43 tendency to saturate in the vicinity of RT. Nevertheless, calculations taking only $i =$
44
45 N , yield both the TEP-curve shape and the above parameters (see Table 2 in Ref. [45
46
47
48
49
50
51
52
53
54
55
56
57
58
59
60
]) close to ours.

Another feature of the here-described $S(T)$ is a change of the sign from
positive to negative at about 75 K, which is easy to explain in the case described

1
2
3 above, *i.e.*, due to the sum of negative $S_d(T)$ and positive $S_{ph}(T)$ contributions. Apart
4
5 from this description, the positive values of S found in the lower temperature region
6
7 may indicate that the principal charge carriers are holes. It also means that the lack of
8
9 charge compensation by the transfer of conduction electrons from uranium to Co and
10
11 Ge atoms creates holes, and only in the high temperature region the electron-type
12
13 conductivity starts to dominate. The large value of S of about $20 \mu\text{V K}^{-1}$ observed for
14
15 UCoGe at $T_{\text{max}} \equiv T_{\text{inf}}$ is attributed to Kondo-lattice type of interactions also reflected
16
17 by fairly large C_p/T values in this region of temperature (see below). At higher
18
19 temperatures $S(T)$ has a tendency to saturate into a large negative value of $-30 \mu\text{V K}^{-1}$.
20
21
22
23
24

25 3.2.3 Thermal conductivity

26
27 Thermal conductivity $\kappa_{\text{tot}}(T)$ data obtained on the annealed sample of UCoGe, taken
28
29 over a range 5 - 300 K, are given in figure 11. This shows that κ_{tot} first increases very
30
31 steeply with rising temperature, then in the vicinity of 25 K it goes through a wide
32
33 knee and finally increases monotonically to RT but having a small anomaly of
34
35 unknown origin around 200 K. At low temperatures up to about 15 K, this
36
37 dependence can be approximated as a linear one. The total thermal conductivity of a
38
39 non-magnetically ordered material as UCoGe is usually expressed as a sum of the
40
41 electronic κ_e and lattice κ_{lat} contributions. At first, we have estimated the contribution
42
43 of the electron thermal conductivity to the total thermal conductivity by using the
44
45 Wiedemann-Franz (W-F) law: $\kappa_e = L_0 T / \rho$, where L_0 is the Sommerfeld value 2.45×10^{-8}
46
47 $\text{W}\Omega \text{K}^{-2}$. As seen from this figure, κ_e is essentially a linear function of temperature
48
49 but having only about 15% value of κ_{tot} at RT. Such a small magnitude of the
50
51 electronic part of the thermal conductivity is caused by large overall values of the
52
53
54
55
56
57
58
59
60

1
2
3 electrical resistivity (see figure 3) being far from that exhibited by typical metallic
4 systems. The steep decrease of the resistivity below 50 K, owing to the coherence
5 effect, is here connected with an almost linear drop of $\kappa_{\text{tot}}(T)$ at the same temperature
6 region. A calculation of the Wiedemann-Franz-Lorenz number $L = \kappa_{\text{tot}}\rho/T$ using the
7 measured thermal conductivity gives abnormal high values for $L(T)$ with a clear
8 evidence that a large lattice term κ_{lat} exists in the total thermal conductivity of
9 UCoGe, several times larger than that of the electronic κ_e one. The temperature
10 dependence of the normalized Lorenz number, L/L_0 , is given in the inset of figure 11.
11 This dependence goes through a well apparent maximum at $T_{\text{max}} \sim 25$ K where this
12 ratio reaches a value of about 18 and then it monotonically declines with further
13 increasing temperature to reach finally at RT a value being 7 times higher than L_0
14 itself. Such a large value at higher temperatures is often an obstacle to observe a
15 Kondo-like behavior in the thermal conductivity [46]. This is possible, however, e.g.
16 for CeCu₂ and YCu₂, also crystallizing in an orthorhombic system like UCoGe, which
17 however show up $L \sim L_0$ [47]. On the other hand, the overall shape of the $L/L_0(T)$
18 function found for UCoGe is very similar to those, e.g. of UPd₂Al₃ [48] or CeCu₂Si₂
19 [49] and other heavy fermion superconductors. Figure 11 shows that separation of the
20 lattice contribution through $\kappa_{\text{lat}} = \kappa_{\text{tot}} - \kappa_e$ yielded the temperature dependence $\kappa_{\text{lat}}(T)$
21 close to that of $\kappa_{\text{tot}}(T)$. Thus, the large Lorenz ratio is due to unusual large ratio $\kappa_{\text{lat}}/\kappa_e$.
22 Furthermore, the lattice component is generally assumed to be composed of several
23 other contributions, like phonon, non-magnetic bipolaron and excitonic ones,
24 depending on the kind of heat carriers [50,51]. Then, the phonon conductivity, κ_{ph}
25 may be described by the Debye model given by Callaway's equation [52] as described
26 in details in Refs. [53] and [54].
27
28
29
30
31
32
33
34
35
36
37
38
39
40
41
42
43
44
45
46
47
48
49
50
51
52
53
54
55
56
57
58
59
60

$$\kappa_{\text{ph}} = GT^3 \int_0^{\Theta/T} \frac{x^4}{\tau^{-1} \sinh^2(x/2)} dx, \quad (2)$$

where $x = \hbar \omega / k_B T$ ($\hbar \omega$ is the phonon energy), G is a constant, Θ_D is the Debye temperature, and τ^{-1} is the sum of inverse relaxation times for various phonon scattering processes [53,54]. In the calculations we have used two parameters, *i.e.*, sound velocity $v_{\text{ph}} = 900 \text{ m/s}$ and Debye temperature $\Theta_D = 250 \text{ K}$. For the other contributions, such as the bipolar (κ_{bip}) and excitonic (κ_{exc}) ones, the heat transport is well described in a review given by Smirnov and Oskotski in Ref. [50].

Figure 11 presents the separation of $\kappa_{\text{lat}}(\text{exp.})$ into $\kappa_{\text{ph}}(\text{calc.})$ and a difference $\Delta\kappa_{\text{lat}}$. It is clearly seen that Callaway's equation well describes the phonon contributions, $\kappa_{\text{ph}}(\text{calc.})$, to κ_{tot} at low temperatures, but above 25 K it diverges from $\kappa_{\text{lat}}(\text{exp.})$ and diminishes with increasing temperature to reach a value at RT as that of κ_e one. The remaining part after the subtraction of $\kappa_{\text{ph}}(\text{calc.})(T)$ from $\kappa_{\text{lat}}(\text{exp.})(T)$, *i.e.*, the difference $\Delta\kappa_{\text{lat}}$, we have assumed to be mainly due to $\kappa_{\text{bip}}(T)$ in such a semimetallic compound as UCoGe. This differential function starting from 25 K follows a shape almost that of high temperature $\kappa_{\text{tot}}(T)$. As we have pointed out in the paper [53], the Callaway equation, however, omits several other possible phonons scattering contributions, *e.g.*, the scattering on the moments in the PM state [50] and hence the difference $\Delta\kappa_{\text{lat}}$ may consist (except for bipolarons) also of other different but difficult to be identified contributions. If we have actually to do with bipolarons in the compound under consideration, a question arises about their role in the occurrence of SC in UCoGe.

3.3 Thermal properties

1
2
3 We show in figure 12(a) the temperature dependences of the specific heat C_p
4 measured up to 180 K for both UCoGe (non-annealed) and ThNiGe; the latter is taken
5 as a non-magnetic reference of the phonon contribution to the total C_p , as it has been
6 done in the case of the transport properties. At lower temperatures, the specific heat
7 over temperature which can be fitted by the equation: $C_p/T = \gamma(0) + BT^2$, where the
8 first and second terms are electronic and phonon contributions, respectively, is shown
9 in the lower inset. The linear response of the above function is apparent for both
10 studied compounds up to 7 K. The values of the electronic specific heat coefficient
11 $\gamma(0)$ and the Debye temperature Θ_D obtained for these two compounds are displayed
12 in this inset. Our $\gamma(0)$ values being of 54 and 7 $\text{mJ K}^{-2} \text{mol}^{-1}$ are close to the literature
13 values of 57 [13] and 5 [55] or 7.6 $\text{mJ K}^{-2} \text{mol}^{-1}$ [31], respectively. The enhancement
14 of the $\gamma(0)$ value by the existence of the 5f-electrons is here almost 8 times.
15 Nevertheless, these values given for UCoGe are not so large compared to those of real
16 heavy-fermion systems (more than 400 $\text{mJ K}^{-2} \text{mol}^{-1}$). On the other hand, the Debye
17 temperature of UCoGe is, as expected, somewhat smaller than that for ThNiGe, *i.e.*,
18 248 against 266 K. The latter value is comparable to 255 K found in Ref. [31] and to
19 246 K reported in Ref. [55]. Despite different crystal structures of these two
20 compounds, the closeness in their Debye temperatures strongly indicates a similarity
21 in their lattice dynamics and justifies using here ThNiGe as a reference non-magnetic
22 compound. The upper inset illustrates the C_p/T vs. T dependences for our two kinds of
23 samples of UCoGe compared to that reported by Huy et al. [13] but in contrast to our
24 results showing the ferromagnetic properties with $T_C \sim 3$ K. It is surprising that our
25 annealed sample, though having no sign of FM order, shows a similar in shape
26 anomaly but being more enhanced as to its magnitude. Certainly both of them do not
27
28
29
30
31
32
33
34
35
36
37
38
39
40
41
42
43
44
45
46
47
48
49
50
51
52
53
54
55
56
57
58
59
60

1
2
3 reveal a λ -type-shape anomaly as expected in the case of the magnetic order. It should
4
5 be noted that our as grown sample although exhibits the low-temperature linear
6
7 behavior in $\rho(T)$, it gives a completely smooth trend in the C_p/T against T curve
8
9 which allowed for a simple extrapolation to $T = 0$ K to get the $\gamma(0)$ value for UCoGe.
10
11 On the other hand, the revealed large hump existing in our low temperature specific
12
13 heat measurements in the annealed sample of UCoGe (see the upper inset of figure
14
15 12 (a)) makes it difficult to judge about any divergent tendency of the C_p/T vs. $\log T$
16
17 function expected for the NFL state, which is well manifested by the observed
18
19 linearity in $\rho(T)$ described above. As seen from this inset, all three considered there
20
21 cases approach the same C_p/T values above 5 K. In addition, there is also shown a
22
23 smooth $C_{ph}(T)$ curve defined as a sum of the Debye and Einstein contributions to C_p
24
25 of ThNiGe, as specified below. This procedure allows to eliminate C_{el} of a given Th-
26
27 compound and signals that C_{ph} is more complex than usual when one uses only the
28
29 Debye function. Thus, in figure 12(b) we display the specific heat difference $\Delta C_p =$
30
31 $C_p - C_{ph}$ plotted against T . We found the difference ΔC_p between these two curves of
32
33 large numbers, being magnetic and electronic in origin. An expected error in ΔC_p is
34
35 usually a sum of errors made during measurements of both heat capacities. To
36
37 minimize the experimental uncertainties in an extraction ΔC_p , we have used as
38
39 $C_{ph}(T)$, i.e. a smooth curve mentioned above, which is without C_{el} of ThNiGe (see
40
41 below).

42
43 As Figure 12(b) indicates, as a result of the above procedure one gets a
44
45 “camel curve”, i.e. there are possible two wide anomalies spanned in the temperature
46
47 range 1.0 – 90 K. Their maxima are centered at about 13 and 45 K and their
48
49 amplitudes are in a rough ratio of about 1:2, respectively. In addition, we present at
50
51
52
53
54
55
56
57
58
59
60

1
2
3 these temperatures the presumably bar errors estimated as ± 5 and ± 2 %, respectively.
4
5 Similar error values have been used by Rietschel et al. [57] in their f-derived ΔC_p for
6
7 a number of magnetically non-ordered uranium and rare-earth compounds as UBe_{13} ,
8
9 UPt_3 , $CeCu_2Si_2$ and $CeCu_6$ showing superconductivity at very low temperatures,
10
11 where they considered the superposition of Kondo and Schottky peaks in these
12
13 compounds, having also to do with subtracting from each other the large numbers.
14
15

16
17 This is well seen in the inset to this figure when subtracting the overall electronic
18
19 specific heat $C_{el}^* = \gamma^* T$ from $\Delta C_p(T)$ of $UCoGe$, but with a gamma value γ^*
20
21 amounting only $\sim 1/3 \gamma(0)$, as presented in figure 12(b). Of course, the temperature
22
23 change in a gamma value from $\gamma(0) = 54.0 \text{ mJ K}^{-2} \text{ molU}^{-1}$ found at $T = 0 \text{ K}$ to a
24
25 constant value $\gamma^* = 18.5 \text{ mJ K}^{-2} \text{ molU}^{-1}$, valid above 90 K, is unknown. However the
26
27 “camel curve” as well as the straight-line $C_{el}^* = \gamma^* T$ are well followed by
28
29 experimental points, which may indicate a good extracting procedure applied and that
30
31 the latter can not be treated as any Schottky contribution. The occurrence of the 13K-
32
33 anomaly seems to be associated with the *crossover* described above in the section
34
35 treated on the transport properties, while that of 45K-one, extended in a wide
36
37 temperature range and having an amplitude about $1.3 \text{ J K}^{-1} \text{ mol}^{-1}$, which is close to
38
39 that expected for $S=1/2$ case of a Kondo-lattice effect C_K [56]. In analogy to the
40
41 situation found for Ce-based compounds, Rietschel *et al.* have analyzed the uranium
42
43 heavy-fermion superconductors: UB_{13} , UPt_{13} , and U_2Zn_{17} in a similar way [57]. The
44
45 value of the determined above amplitude is several time too small to ascribe it to a
46
47 Schottky-type anomaly. For uranium compounds, due to usually large splittings of the
48
49 CEF levels one cannot expect such a well defined anomaly peak (e.g. see Ref. [58]).
50
51 Taking into account the fact reported by Desgranges and Schotte [56] that $T_{max} = 0.45$
52
53
54
55
56
57
58
59
60

1
2
3 T_K , where T_K is a Kondo temperature, one finds T_K for UCoGe being equal to about
4
5 100 K. This value is just equal to about $2 T_{coh}$. In addition, the temperature variation
6
7 of the magnetic entropy, S_m , is shown in the inset of figure 12(b). At 100 K S_m is
8
9 equal to about $0.3R\ln 2$.

10
11
12 Moreover, in figure 13 the C_p vs. T curve is drawn separately for ThNiGe
13
14 which may allow to perform an analysis of the lattice contribution to the total $C_p(T)$
15
16 dependence just in UCoGe, assuming that for this aim the Th-based compound as a
17
18 non-magnetic reference may be used. As seen from this figure, only by combining the
19
20 Debye and Einstein modes together **with the electronic heat contribution** we could fit
21
22 fairly well the experimental data, **by a smooth curve through the experimental points,**
23
24 **mentioned above. Due to this fitting we got a little higher overall γ_{ht} than $\gamma(0)$.**
25
26 **However,** no satisfactory agreement between the fitting results and the experimental
27
28 data has been obtained (not shown) using only the Debye approach. This is better
29
30 apparent in figure 14 where we have plotted the C_p/T^3 against T dependence for both
31
32 ternaries considered here. It is well seen there that the low-temperature Einstein
33
34 modes in the lattice heat do exist undoubtedly (see the appropriate maximum at T_{max}
35
36 for the Th-based material, while for the U-based one there is only a marked hump
37
38 centered at the same T_{max} being less apparent due to a large value of the electronic
39
40 specific heat contribution found for the latter compound). This supports again the fact
41
42 that the lattice dynamics of both these compounds are similar to each other. From
43
44 rough fitting (solid line) we have obtained the approximate weighted equation,
45
46 displayed in this figure, where $C_D(C_E)$ represents the specific heats due to the Debye
47
48 (Einstein) phonons (involving the total nine expected modes, *i.e.*, three acoustic and
49
50 six optic modes) and with the electronic term C_{el} also added. **The** corresponding
51
52
53
54
55
56
57
58
59
60

1
2
3 values of the characteristic temperatures Θ_D and Θ_E are also given in this figure. It is
4
5 thus clear from the above formula that for the best possible fitting, the lattice heat is
6
7 found to require about seven oscillators per f.u. for the Debye phonons and about two
8
9 oscillators per f.u. for the Einstein low-lying optic phonons. This procedure is taken
10
11 from Ref. [59] where the case of YbGaGe was analyzed. Of course, as mentioned
12
13 already above, the fitted electronic contribution is here represented by a high
14
15 temperature coefficient, γ_{ht} , which is a little bit higher than $\gamma(0)$ of ThNiGe.
16
17
18
19
20

21 4. Conclusions

22
23 Our results of bulk measurements done on an annealed single crystal show
24
25 superconductivity but do not reproduce the previously reported coexistence with
26
27 ferromagnetism. The magnetization studies, however, show the presence of low-
28
29 temperature strong ferromagnetic correlations in UCoGe, possibly due to the
30
31 proximity of this compound into the quantum critical point. The recent paper by
32
33 Slooten et. al. [18] has shown that near the ferromagnetic critical point $p_c= 1.4$ GPa
34
35 superconductivity is not only enhanced but also it is still present in the paramagnetic
36
37 region induced by higher pressures. Thus, this result clearly indicates again the
38
39 possibility for UCoGe to show up superconductivity without weak FM order.
40
41
42
43

44
45 The most essential to underline here is the fact that the electrical resistivity
46
47 data exhibit a linear behavior at low temperatures for our non-magnetic sample of
48
49 UCoGe being followed by the coherence-type knee in $\rho(T)$ at around 50 K and then at
50
51 much higher temperatures this dependence reveals a single-ion Kondo-like effect. In
52
53 turn, the transverse magnetoresistivity contains only a negative contribution in its
54
55 field and temperature dependences in the whole range of the paramagnetic state of
56
57
58
59
60

1
2
3 UCoGe and by this the presence of the Kondo-like state is confirmed in this
4
5 germanide at higher temperatures. This state is also reflected by the corresponding
6
7 high temperature Kondo- peak in the specific heat. The positive extremum in
8
9 thermoelectric power, the maxima in the temperature derivatives of the resistivity and
10
11 magnetoresistivity and also a low-temperature anomaly in the specific heat, all these
12
13 occur almost at the same temperature of around 13 K. Thus, this temperature gives
14
15 rise to the *crossover* transition in UCoGe from a more localized behavior of the 5f-
16
17 electron states in the higher temperature region and, hence, the appearance of a
18
19 Kondo-like effect to a more metallic state in the lower temperature region allowing
20
21 for the superconductivity. Finally, the measured thermal conductivity points to the fact
22
23 of a predominant role of the lattice contribution in UCoGe, which may play some
24
25 special role in both the exhibited superconductivity and thermopower behavior.
26
27 Nevertheless, the remarkable large values of the upper critical field $B_{C2}(0)$ provides
28
29 evidence for spin-triplet superconductivity which persists in the paramagnetic phase
30
31 of the considered here germanide [18].
32
33
34
35
36
37
38
39

40 Acknowledgments

41 We are grateful to B. Coqblin for his interest in this paper and E. Talik for synthesizing the single
42 crystal. Technical assistance of G. Badurski and R. Gorzelniak with some experiments as well as a
43 fitting of the thermal conductivity by J. Mucha are acknowledged.
44

45 References

- 46
47 [1] R. Troć and V.H. Tran, J. Magn. Magn. Mater. 73 (1988) p. 389.
48 [2] F.R. de Boer, E. Brück, V. Sechovský, L. Havela and K.H.J. Buschow, Physica B 163 (1990) p.
49 175.
50 [3] L. Havela, A. Kolomiets, V. Sechovský, M. Diviš, M. Richter and A.V. Andreev, J. Magn. Magn.
51 Mater 177-181 (1998) p. 47.
52 [4] K.H.J. Buschow, E. Brück, R.G. van Wierst, F.R. de Boer, L. Havela, V. Sechovský, P. Nozar, E.
53 Sugiura (M. Ono, M. Date and Y. Yamagishi, J. Appl. Phys. 67 (1990) p. 5215.
54 [5] G.G. Lonzarich, in *Electron: A Centenary Volume*, M. Springford, ed., Cambridge Univ. Press
55 Cambridge 199, Chap. 6 &
56 [6] E. Diviš, Physica B 403 (2008) p. 2505.
57 [7] P. de la Mora and O. Lavarro J. Phys.: Condens. Matter 20 (2008) p. 285221.
58 [8] M. Samsel-Czekala, S. Elgazzar, P.M. Oppeneer, E. Talik, W. Walerczyk and R. Troć, J. Phys.
59
60

- Condens. Matter. **22** (2010) p. 015503.
- [9] FPLO-5.00-18 and 5.10-20 [improved version of the original FPLO code by K. Koepernik and H. Eschrig, Phys. Rev. B 59 (1999) p. 1743]; <http://www.FPLO.de>.
- [10] N.T. Huy, A. Gasparini, D.E. de Nijs, Y. Huang, J.C.P. Klaasse, T. Gortenmulder, A. de Visser, A. Hamann, T. Görlach and H. v. Löhneysen, Phys. Rev. Lett. 99 (2007) p. 067006.
- [11] S. Sakarya, N.T. Huy, N.H. van Dijk, A. de Visser, M. Wagemaker, A.C. Moleman, T.J. Gortenmulder, J.C.P. Klaasse, M. Uhlarz and H. v. Löhneysen, J. Alloys Compd. 457 (2008) p. 51.
- [12] D.E. de Nijs, N.T. Huy and A. de Visser, Phys. Rev. B 77 (2008) p. 140506(R).
- [13] N.T. Huy, D.E. de Nijs, Y.K. Huang and A. de Visser, Phys. Rev. Lett. 100 (2008) p. 077002.
- [14] E. Hassinger, D. Aoki, G. Knebel and J. Flouquet, J. Phys. Soc. Jpn. 77 (2008) p. 073703.
- [15] A. de Visser, N.T. Huy, A. Gasparini, D.E. de Nijs, D. Andreica, C. Baines and A. Amato, Phys. Rev. Lett. 102 (2009) p. 167003.
- [16] T. Ohta, Y. Nakai, Y. Ihara, K. Ishida, K. Deguchi, N. K. Sato and I. Satoh, J. Phys. Soc. Jap. 77 (2008) p. 023707.
- [17] N.T. Huy, Y.K. Huang and A. de Visser, J. Magn. Magn. Mater. 321 (2009) p. 2691.
- [18] E. Slooten, T. Naka, A. Gasparini, Y.K. Huang and A. de Visser, Phys. Rev. Lett. 103 (2009) p. 097003.
- [19] R. Wawryk and Z. Henkie, Phil. Mag. B 81 (2001) p. 223.
- [20] Z. Henkie and R. Wawryk, Solid State Commun. 122 (2002) p. 1.
- [21] J.P. Perdew and Y. Wang, Phys. Rev. B 45 (1992) p. 13244.
- [22] V. Sechovsky, L. Havela, F.R. de Boer, J.J.M. Franse, P.A. Veenhuizen, J. Sebec, J. Stechno, A.V. Andreev, Physica 142B (1986) p. 283.
- [23] V.H. Tran, R. Troć, H. Noël, J. Alloys Compd. 262-264 (1997) p. 471.
- [24] D. Kaczorowski, H. Noël, J. Phys.: Condens. Matter 5 (1993) p. 9185.
- [25] N.T. Huy and A. de Visser, Solid State Commun. 149 (2009) p. 703.
- [26] T.D. Matsuda, D. Aoki, S. Ikeda, E. Yamamoto, Y. Haga, H. Ohkuni, R. Settai and Y. Ōnuki, Proc. J. Phys. Soc. Jpn. 77, Suppl A (2008) p. 362.
- [27] D. Aoki, Y. Haga, T.D. Matsuda, S. Ikeda, Y. Homma, H. Sakai, Y. Shiokawa, E. Yamamoto, N. Nakamura, R. Settai and Y. Ōnuki, J. Phys.: Condens. Matter 21 (2009) p. 164203.
- [28] W. Miiller and V.H. Tran, Acta Phys. Pol. A 115 (2009) p. 144.
- [29] D.R. Grempel and M.J. Rozenberg, Phys. Rev. B 60 (1999) p. 4702.
- [30] N.T. Huy, A. Gasparini, J.C.P. Klaasse, A. de Visser, S. Sakarya and N.H. Van Dijk, Phys. Rev. B. 75 (2007) p. 212405.
- [31] P. Manfrinetti, A. Palenzona, S.K. Dhar and C. Mitra, Intermetallics 7 (1999) p. 1291.
- [32] As an example, see J.S. Schilling, Phys. Rev. B 33 (1986) p. 1667.
- [33] N.F. Mott, Proc. Roy. Soc. 156 (1936) p. 368.
- [34] T.T.M. Palstra, A.A. Menovsky and J.A. Mydosh, Phys. Rev. B 33 (1986) p. 6527.
- [35] F. Canepa, P. Manfrinetti, M. Pani and A. Palenzona, J. Alloys Compd. 234 (1996) p. 225.
- [36] V. Zlatić, T.A. Costi, A.C. Hewson and B.R. Coles, Phys. Rev. B 48 (1993) p. 16152; D.L. Cox and N. Grewe, Z. Phys. B 71 (1988) p. 321.
- [37] F.J. Blatt, in *Physics of Electronic Conduction in Solids*, McGraw-Hill, New York, 1968.
- [38] A. de Visser, J.J.M. Franse and A. Menovsky, J. Magn. Magn. Mater. 43 (1984) p. 43.
- [39] F. Steglich, U. Rauchschwalbe, U. Gottwick, H.M. Mayer, G. Sparm, N. Grewe, U. Poppe and J.J.M. Franse, J. Appl. Phys. 57 (1985) p. 3054.
- [40] T. Takabatake, S. Miyata, H. Furi, Y. Aoki, T. Suzuki, T. Fujita, J. Samuraj and T. Hiraoka, J. Phys. Soc. Jpn. 59 (1990) p. 4412.
- [41] U. Gottwick, K. Gloos, S. Horn, F. Steglich and N. Grewe, J. Magn. Magn. Mater. 47-48 (1985) p. 536.
- [42] F.J. Blatt, P.A. Schroeder, C.L. Foiles and D. Greig, *Thermoelectric Power of Metals*, Plenum, New York, 1976, p. 147, and references therein.
- [43] R. Troć, Z. Bukowski, C. Sułkowski, H. Misiorek, J.A. Morkowski, A. Szajek and G. Chełkowska, Phys. Rev. B 70 (2004) p. 184443.
- [44] H.J. Trodahl, Phys. Rev. B 51 (1995) p. 6175.
- [45] Y. Bando, T. Suemitsu, K. Takagi, H. Tokushima, Y. Echizen, K. Katoh, K. Umeo, Y. Maeda and T. Takabatake, J. Alloys Compd. 313 (2000) p. 1.

- [46] E. Bauer, E. Gratz, G. Hutflesh, A.K. Bhattacharje and B. Coqblin, *J. Mag. Mag. Mater.* 108 (1992) p. 159.
- [47] E. Gratz, E. Bauer, B. Barbara, S. Zemirli, F. Steglich, C.D. Bredl and W. Lieke, *J. Phys. F: Metal Phys.* 15 (1985) p. 1975.
- [48] M. Hiroi, M. Sera, N. Kobayashi, Y. Haga, E. Yamamoto and Y. Onuki, *J. Phys. Soc. Jpn.* 66 (1997) p. 1595.
- [49] W. Franz, A. Griebel, F. Steglich and D. Wohlleben, *Z. Phys. B* 31 (1978) p. 7.
- [50] I.A. Smirnov and V.S. Oskotski, in *Handbook on the Physics and Chemistry of Rare Earths*, Vol. 16, K.A. Gschneidner and L. Eyring, eds., North Holland, Amsterdam 1993, p. 116.
- [51] R. Berman, in *Thermal Conductivity in Solids*, Carendon, Oxford, 1976.
- [52] J. Callaway, *Phys. Rev.* 113 (1959) p. 1046.
- [53] J. Mucha, H. Misiorek, R. Troć and B. Coqblin, *J. Phys.: Condens. Matter* 20 (2008) p. 085205.
- [54] J. Mucha, H. Misiorek, R. Troć and Z. Bukowski, *J. Phys.: Condens. Matter* 18 (2006) p. 3097.
- [55] S. Kawamata, H. Iwaszki and N. Kobayashi, *J. Magn. Mater.* 104-107 (1992) p. 55.
- [56] H.U. Desgranges and K.D. Schotte, *Phys. Lett.* 91A (1982) p. 240.
- [57] H. Rietschel, B. Renker, R. Felten, F. Steglich and G. Weber, *J. Magn. Mater.* 76-77 (1988) p. 105.
- [58] G. Amoretti, A. Blaise, J.M. Collard, R.O.A. Hall, M.J. Mortimer and R. Troć, *J. Magn. Mater.* 46 (1984) p. 57.
- [59] K-H. Jang, W-Y Song, J.-G. Park, H.C. Kim, A. Lindbaum, H. Müller and E. Bauer, *Europhys. Lett.* 69 (2005) p. 88.

Figure captions

Figure 1. (Color online) **Part (a):** Magnetic susceptibility χ_i against temperature for as grown and annealed samples of UCoGe. The inset shows the isothermal magnetization M vs. an applied magnetic field. **Part (b): Arrott plot of magnetisation isotherms corresponding to M curves displayed in the inset to part (a).**

Figure 2. (Color online) The inverse magnetic susceptibility χ^{-1} of the UCoGe crystal measured along two directions (indicated) as a function of temperature. The insets show the magnetization M against both temperature T (upper one) and applied magnetic fields B at 1.72 K (lower one) for both crystallographic directions. The latter was measured in increasing (open symbols) and decreasing (solid symbols) fields.

Figure 3. (Color online) Electrical resistivity $\rho(T)$ curves for as grown and annealed samples of UCoGe. Left hand inset shows the low temperature behavior of $\rho(T)$, and right hand one presents the temperature derivative $d\rho(T)/dT$ of the resistivity.

Figure 4. (Color online) The low temperature resistivity on the expanded temperature scale.

Figure 5. (Color online) The determination of the differential resistivity $\Delta\rho_{1,2}$ ($= \Delta\rho_1 - \Delta\rho_2$) against temperature for the annealed sample of UCoGe after subtracting the phonon reference data based on ThNiGe.

Figure 6. (Color online) The differential resistivity $\Delta\rho_{1,2}$ ($= \Delta\rho_1 - \Delta\rho_2$) as in figure 5 vs. temperature on a logarithmic scale. The inset displays a fitting of the experimental resistivity taken for ThNiGe to the Bloch-Grüneisen-Mott equation [33].

1
2
3
4
5
6
7
8
9
10
11
12
13
14
15
16
17
18
19
20
21
22
23
24
25
26
27
28
29
30
31
32
33
34
35
36
37
38
39
40
41
42
43
44
45
46
47
48
49
50
51
52
53
54
55
56
57
58
59
60

Figure 7. (Color online) The low-temperature dependences of the resistivity in $B=0$ and 8 T (a) and **their transverse** magnetoresistivity $\Delta\rho/\rho_0(T)$ at $B=8$ T (b) for the annealed sample of UCoGe. The insets illustrate the Fermi-liquid behavior of the resistivity measured at 8 T (a) and the temperature derivative of the magnetoresistivity, $d(\Delta\rho/\rho_0(T))/dT$, at $B=8$ T (b). T_{inf} ($=13$ K) is the characteristic temperature of the *crossover* (see text). The solid squares indicate the values of TMR taken from figure 8 at 8 T.

Figure 8. (Color online) Transverse magnetoresistivity against applied magnetic fields $\Delta\rho/\rho_0(B)$ up to 8 T measured at various temperatures 4.2 – 40 K. The dashed curves depict the square B^2 field dependencies. In the inset the coefficient α is plotted against T .

Figure 9. (Color online) Measured (symbols) and calculated (dashed line) TEP for UCoGe. The upper inset shows the low temperature $S(T)$ dependences for two samples of UCoGe: as grown and annealed (open and solid circles, respectively) and, additionally, the first temperature derivative of $S(T)$ for the latter sample (squares). One can see from this inset an almost linear variation of $S(T) = \alpha T$ below about 2.5 K. The lower inset displays a fitting of the phenomenological modified Mott equation to the low temperature variation of $S(T)$.

Figure 10. (Color online) The calculated two parts of densities of states **DOS** in paramagnetic UCoGe, *i.e.*, $N_s(E)$ and $N_{pdf}(E)$, defined in the text. The insert shows the energy derivative of $N_{pdf}(E)$ drawn in the enlarged scale around E_F .

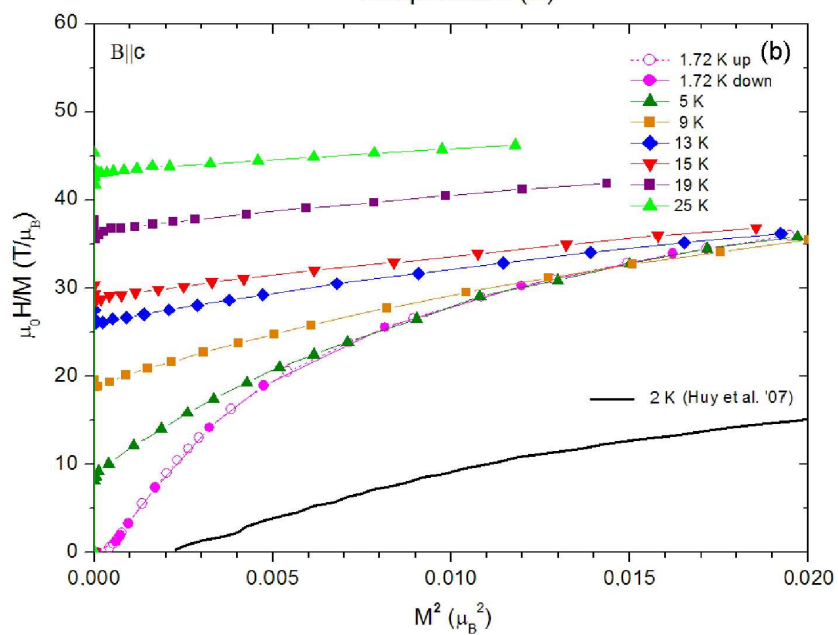
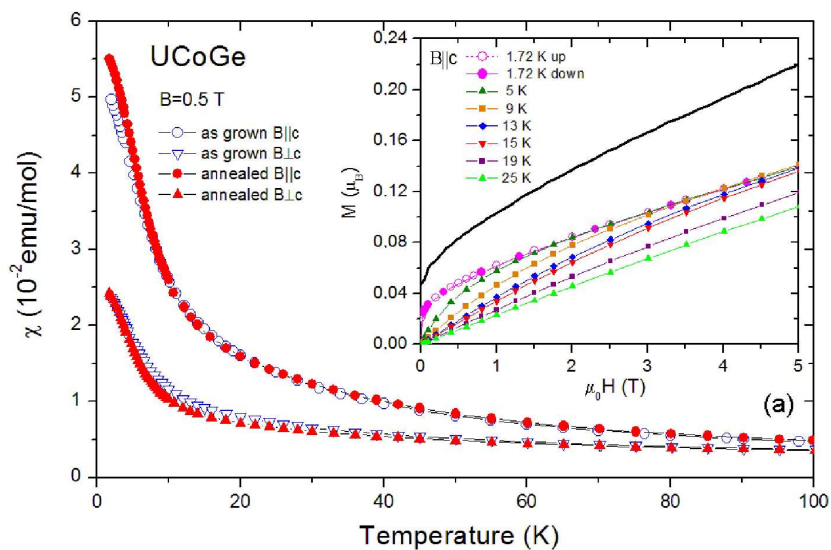
Figure 11. (Color online) Thermal conductivity κ_{tot} vs. T (squares). After using the W-F law and making separation of κ_{tot} , we obtained its two main contributions: electronic κ_e (dotted curve) and lattice $\kappa_{\text{lat}}(\text{exp.})$ (circles) parts, respectively. The dashed line presents the difference $\Delta\kappa_{\text{lat}}$ obtained by extracting from $\kappa_{\text{lat}}(\text{exp.})$ the $\kappa_{\text{ph}}(\text{calc.})$ part (solid line) based on the Calleway model which is discussed in the text. The inset shows the normalized L/L_0 ratio vs. T .

Figure 12. (Color online) Part (a): Specific heat C_p vs. T for UCoGe and the reference compound ThNiGe **as well as the simulated $C_{\text{ph}}(T)$ function, based on the latter compound**. The lower and upper insets show, the low-temperature C_p/T vs. T^2 curves for both compounds and C_p/T vs. T dependencies for only UCoGe, respectively. Part (b) The difference $\Delta C_p = C_p(\text{UCoGe}) - C_{\text{ph}}$ **depending on T , as specified in the text**. In the inset the same dependence is displayed but with the high temperature electronic specific heat ($C_{\text{el}} = \gamma^* T$) being subtracted. In addition, the temperature variation of the magnetic entropy S_m **of U 5f electrons** is **also** presented (solid line).

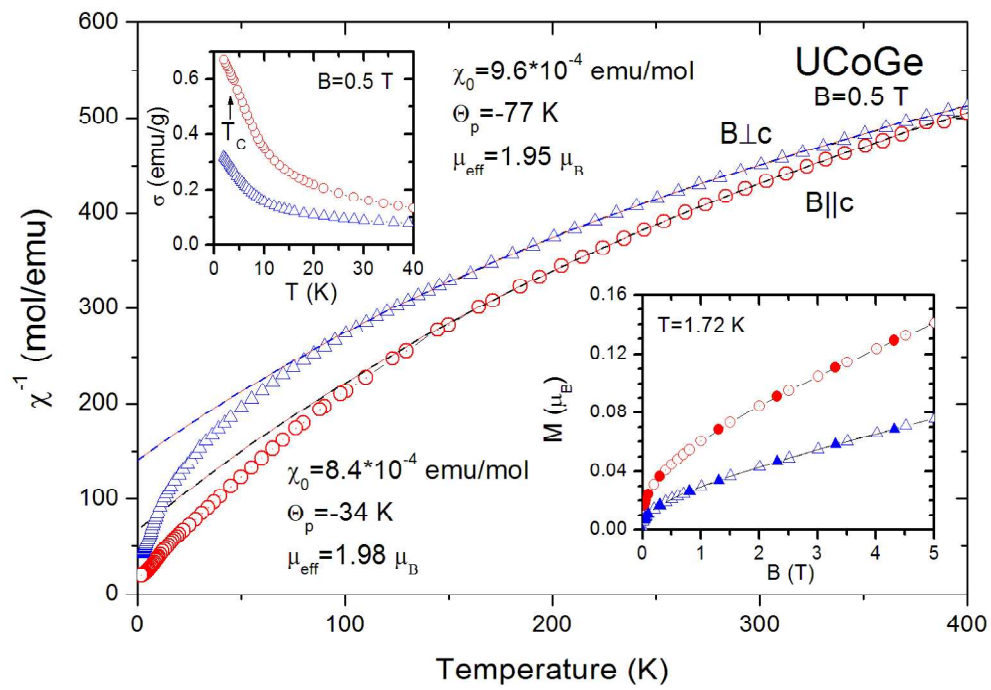
Figure 13. (Color online) Total specific heat C_p measured for ThNiGe (solid circles). A deconvolution of the total C_p into the Debye (C_D), Einstein (C_E), and electronic (C_{el}) specific heat contributions is also presented **as C_{fit} (solid line)**. **The two former contributions define the smooth $C_{\text{ph}}(T)$ curve, shown in figure 12(a)**. **The fitting parameters shown in the figure are described in the text**.

1
2
3
4
5 Figure 14. (Color online) The C_p/T^3 vs. T plot presents all the specific heat
6 contributions into C_p of ThNiGe, described in figure 13 and additionally such a total
7 plot for UCoGe.
8
9
10
11
12
13
14
15
16
17
18
19
20
21
22
23
24
25
26
27
28
29
30
31
32
33
34
35
36
37
38
39
40
41
42
43
44
45
46
47
48
49
50
51
52
53
54
55
56
57
58
59
60

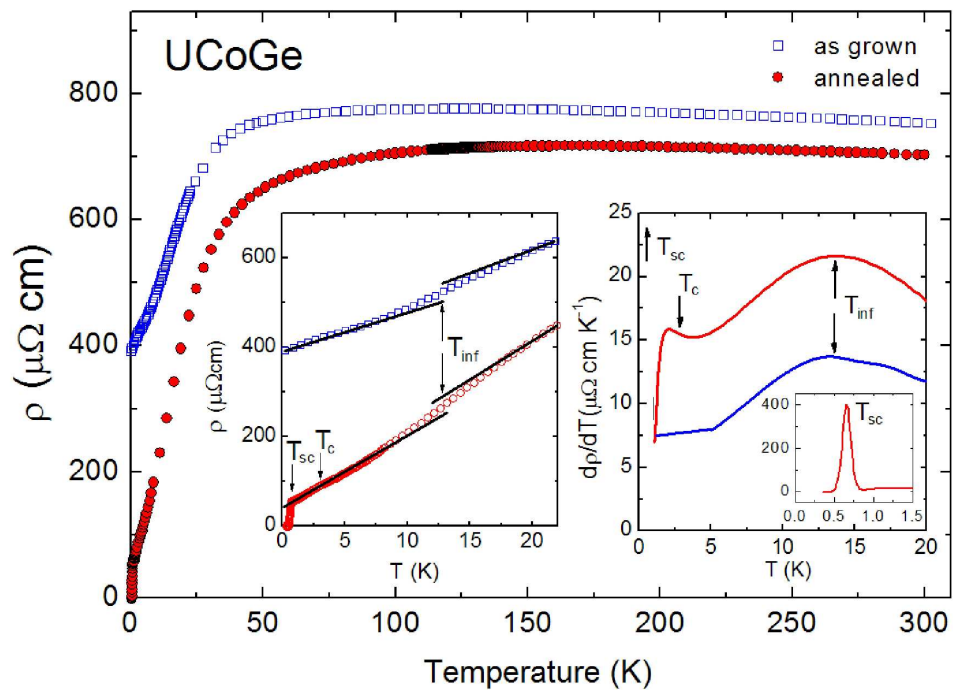
For Peer Review Only



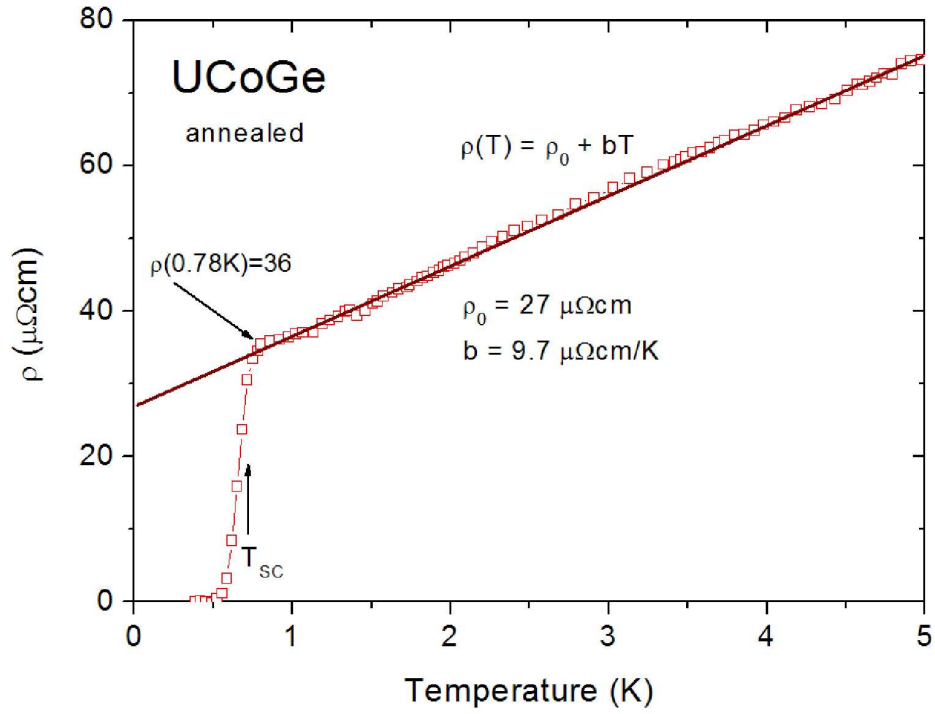
378x519mm (600 x 600 DPI)



555x391mm (600 x 600 DPI)

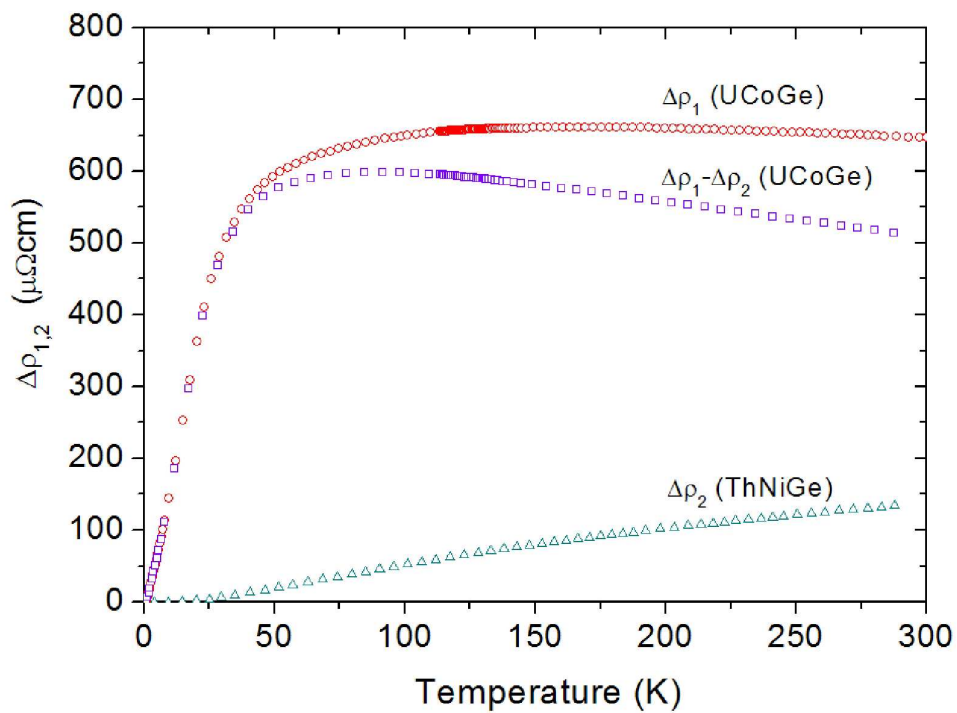


1
2
3
4
5
6
7
8
9
10
11
12
13
14
15
16
17
18
19
20
21
22
23
24
25
26
27
28
29
30
31
32
33
34
35
36
37
38
39
40
41
42
43
44
45
46
47
48
49
50
51
52
53
54
55
56
57
58
59
60



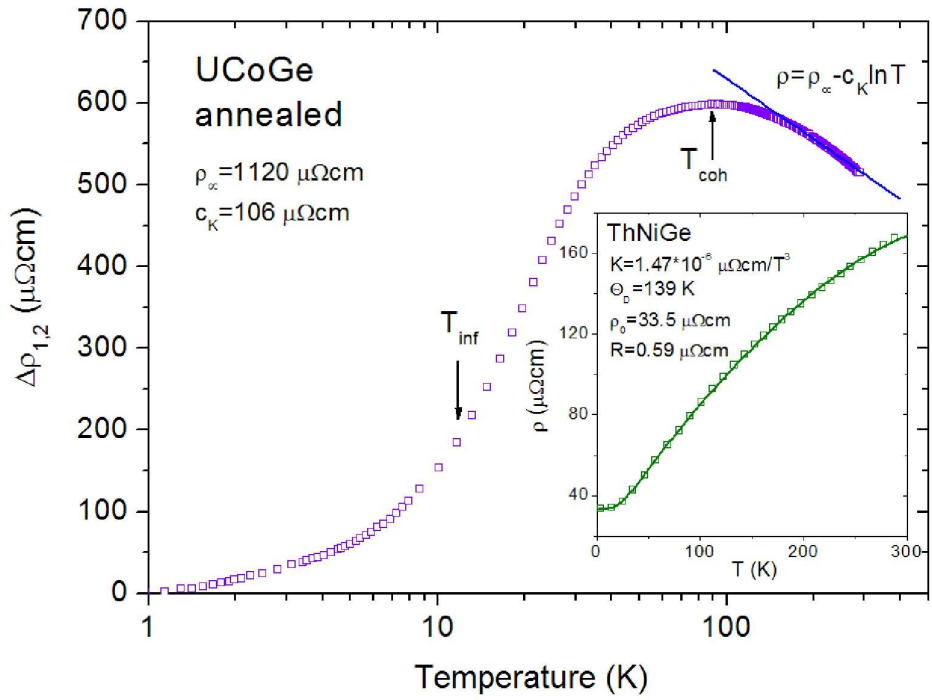
345x268mm (600 x 600 DPI)

Pre-proof Only



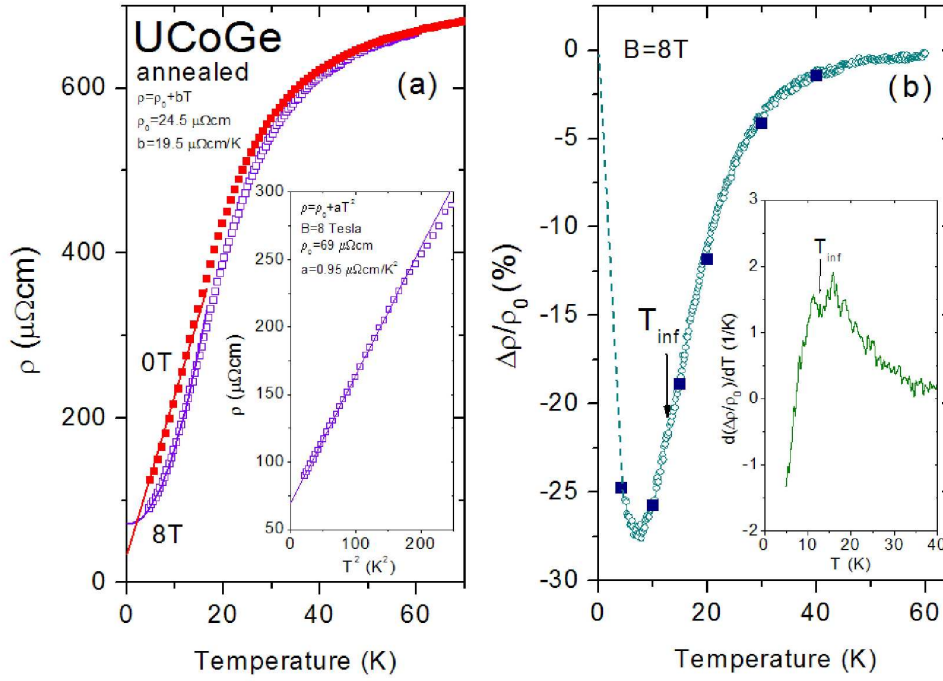
349x264mm (600 x 600 DPI)

1
2
3
4
5
6
7
8
9
10
11
12
13
14
15
16
17
18
19
20
21
22
23
24
25
26
27
28
29
30
31
32
33
34
35
36
37
38
39
40
41
42
43
44
45
46
47
48
49
50
51
52
53
54
55
56
57
58
59
60



350x261mm (600 x 600 DPI)

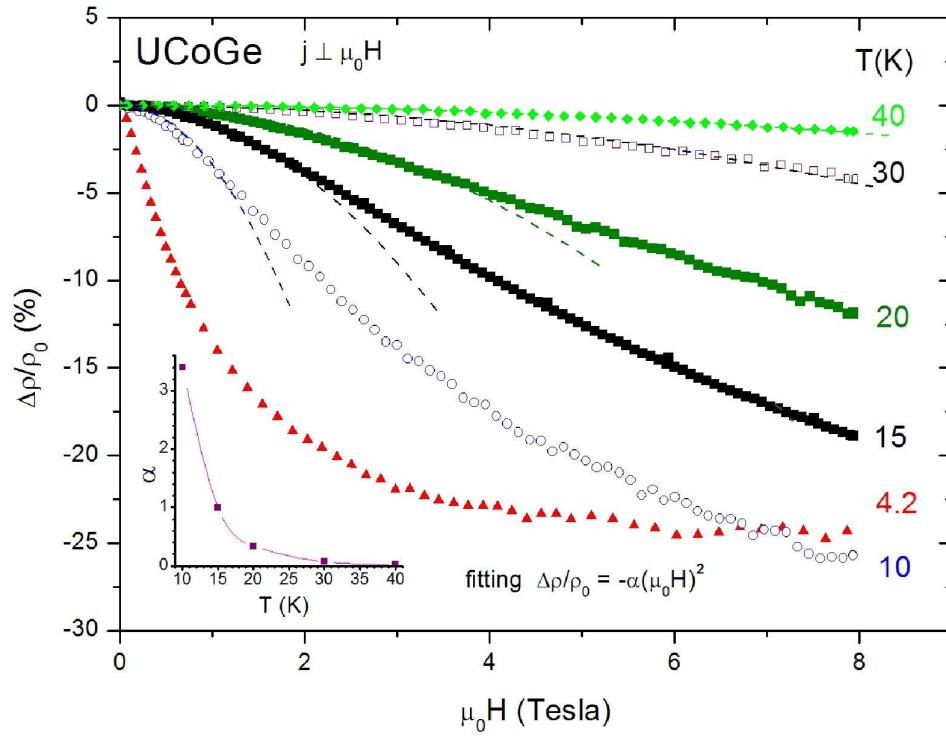
new Only



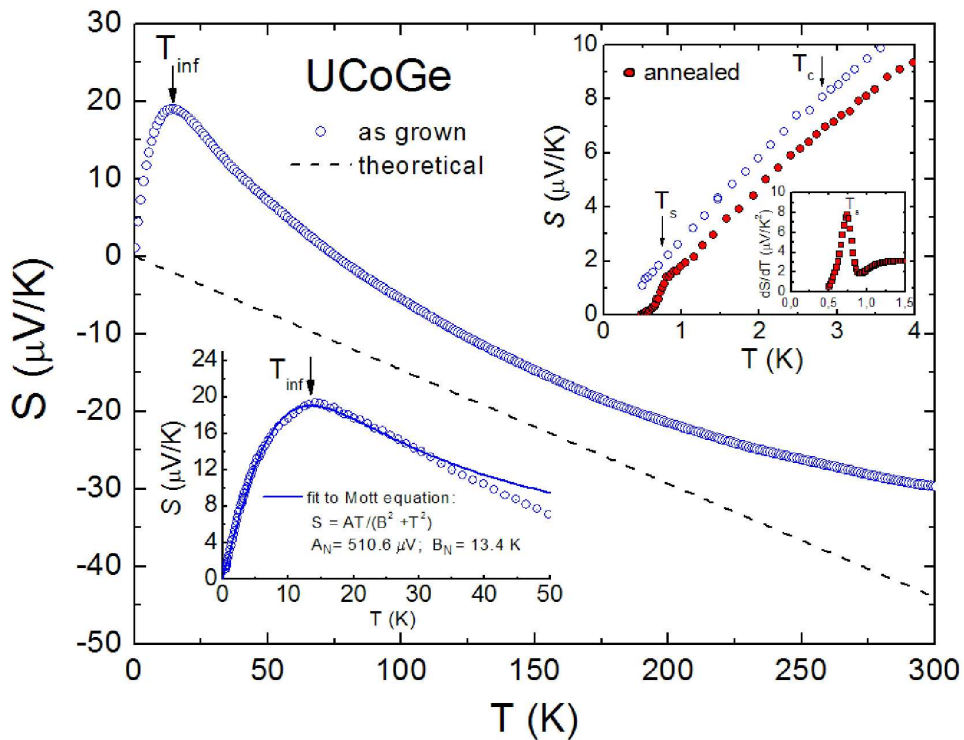
362x264mm (600 x 600 DPI)

new Only

1
2
3
4
5
6
7
8
9
10
11
12
13
14
15
16
17
18
19
20
21
22
23
24
25
26
27
28
29
30
31
32
33
34
35
36
37
38
39
40
41
42
43
44
45
46
47
48
49
50
51
52
53
54
55
56
57
58
59
60

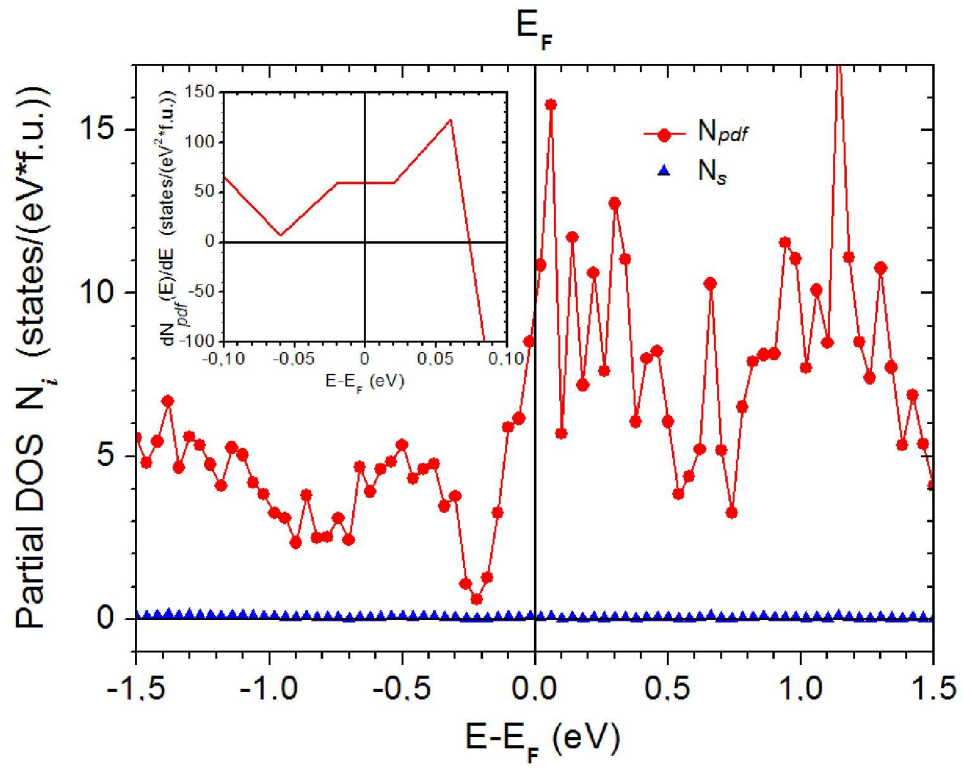


492x384mm (600 x 600 DPI)



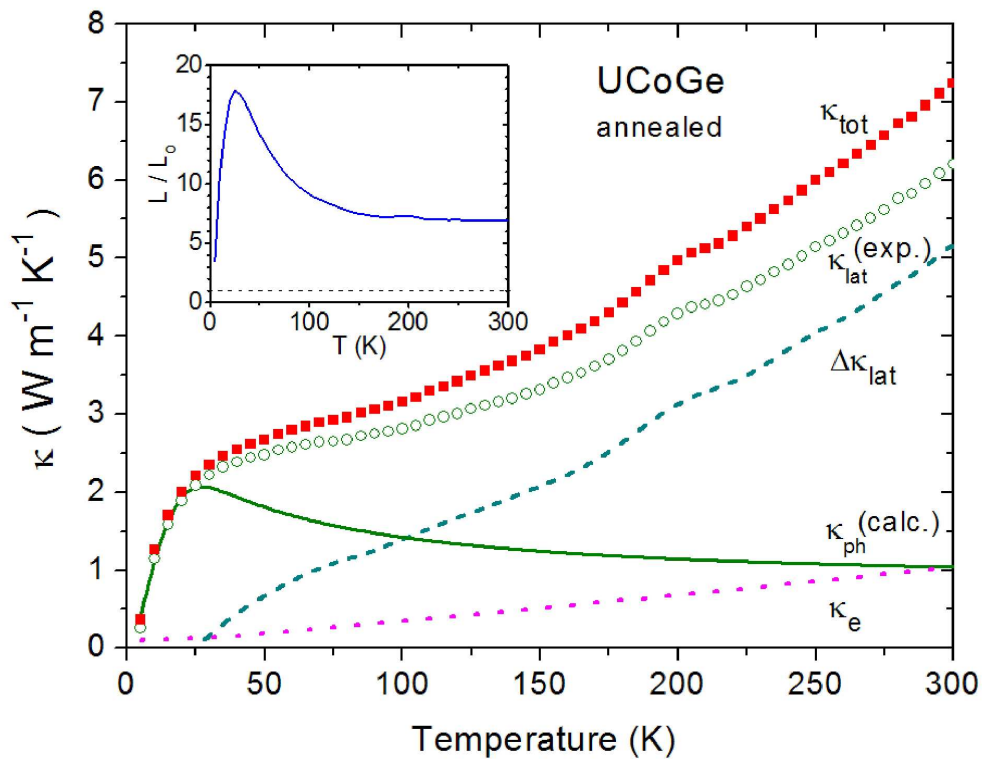
369x287mm (600 x 600 DPI)

1
2
3
4
5
6
7
8
9
10
11
12
13
14
15
16
17
18
19
20
21
22
23
24
25
26
27
28
29
30
31
32
33
34
35
36
37
38
39
40
41
42
43
44
45
46
47
48
49
50
51
52
53
54
55
56
57
58
59
60

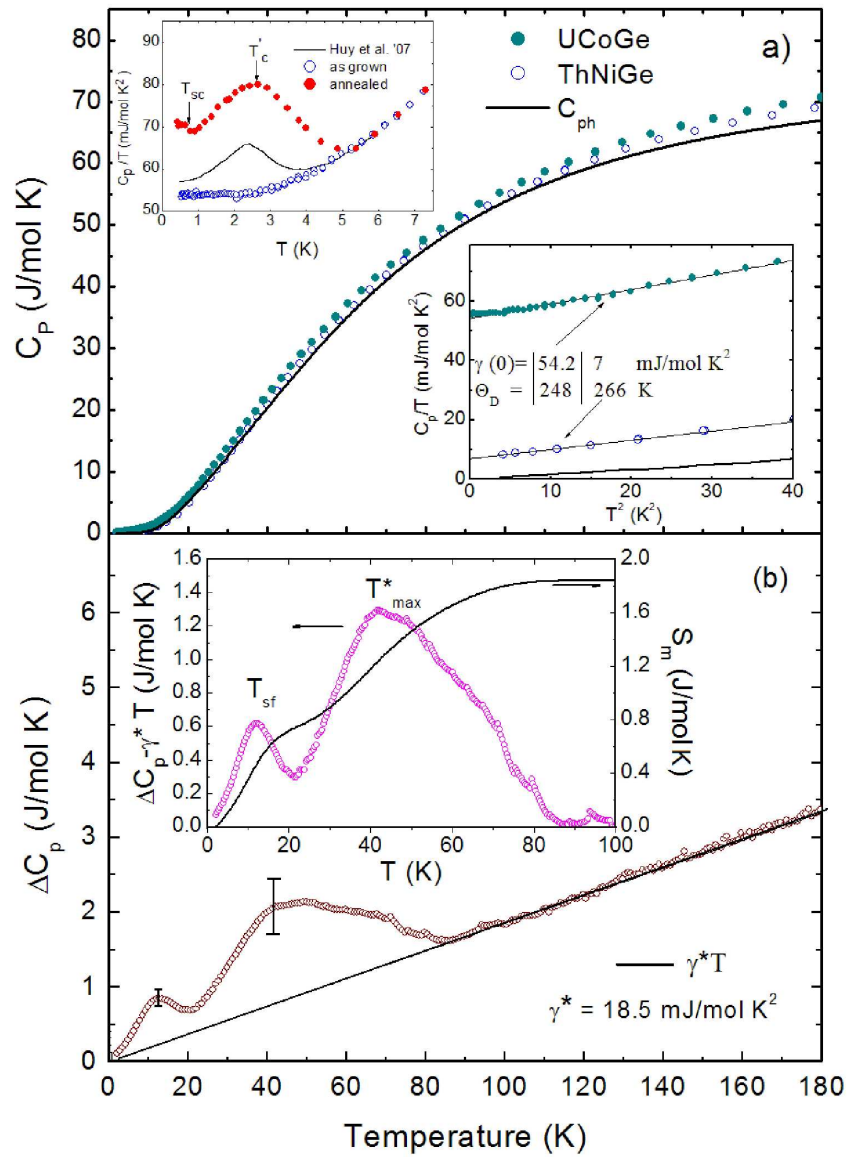


337x269mm (600 x 600 DPI)

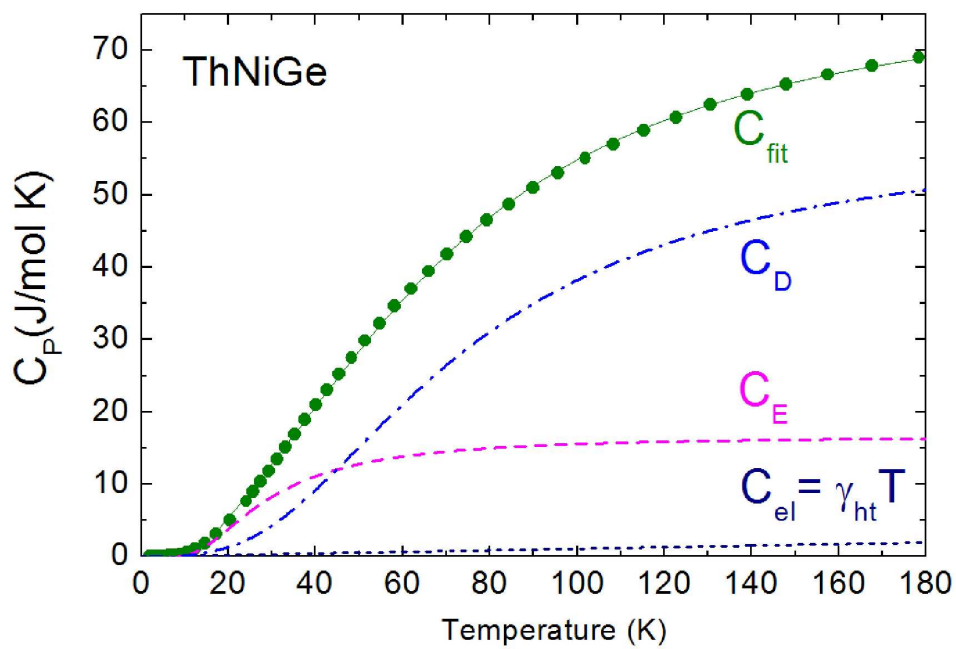
View Only



324x261mm (600 x 600 DPI)

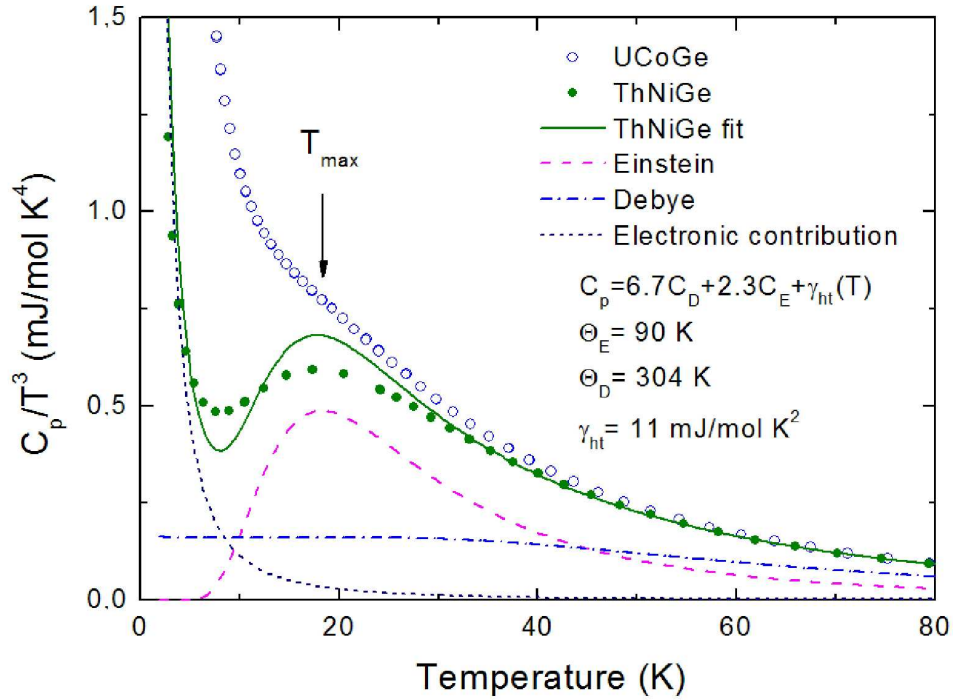


334x459mm (600 x 600 DPI)



382x267mm (600 x 600 DPI)

view Only



344x259mm (600 x 600 DPI)